PHYSICAL REVIEW C VOLUME 43, NUMBER 1 JANUARY 1991

Angular momentum and incident-energy dependence of nucleus-nucleus interaction

Shinichiro Yamaguchi
Yukawa Institute for Theoretical Physics, Kyoto University, Kyoto 606, Japan
(Received 30 August 1990)

The purpose of this paper is to understand intuitively the origin of the angular momentum and incident-energy dependence of the nucleus-nucleus interaction on the basis of the totally- antisymmetrized many-body theory. With the aim of understanding the structure of the nucleus-nucleus interaction, we show first that the nucleus-nucleus interaction can be written by the use of the density-distribution function and the phase-space distribution function instead of using the many-body wave function itself. And we show that the structure change of the density-distribution function with the increase of the angular momentum causes the angular momentum dependence of the nucleus-nucleus interaction and that the incident-energy dependence of the nucleus-nucleus interaction originates from the structure change of the phase-space distribution function.

I. INTRODUCTION

The angular momentum and incident-energy dependence are basic characteristics of the nucleus-nucleus interaction. One of the origins of these characteristics is the fact that the nucleus is a composite particle of fermions and so total antisymmetrization is required. Until now by use of the microscopic studies with the resonating-group method (RGM) and its semiclassical version (RGM+WKB), it has been made obvious that the total antisymmetrization of the nucleon wave functions gives rise to this character.[1,2]

In addition to the antisymmetrization, there are some other origins, such as dynamical polarization, to endow this property to the nucleus-nucleus interaction. As for the incident-energy dependence caused by the dynamical polarization, it is easy to understand the structure of it if we neglect the nonlocality. On the other hand, though it is already known that the antisymmetrization brings the angular momentum and incident-energy dependence to the nucleus-nucleus interaction, it cannot be said that the structure of this dependence is clearly understood.

The purpose of this paper is to get intuitive understandings of the angular momentum and incident-energy dependence caused by the antisymmetrization. Especially we discuss this property from the viewpoint of the structure change of nucleon distribution functions. The distribution functions mentioned here are the density-distribution function and the phase-space distribution function (Wigner function). These functions give us the most intuitive information on the mode of existence of the nucleus-nucleus system.

The above-mentioned nature of the nucleus-nucleus interaction is also caused by the state dependence and the structure dependence (density dependence and starting-energy dependence) of the nucleon-nucleon effective interaction. This time, however, we pay attention only to the effects of the antisymmetrization. In this paper we employ a many-body theory employing a totally antisymmetrized wave function and an effective interaction which is density- and starting-energy independent.

The many-body theory employed here is the canonical moving wave-packet method (CMWP).[3,4] This method describes the internucleus relative motion in a semiclassical way on the basis of the time-dependent variational principle.[5] As for the reliability of this method, it has already shown that the internucleus potential obtained by this method coincides well with the one by more reliable RGM+WKB.[4,6]

The many-body wave function used in CMWP is a single Slater determinant of the harmonic-oscillator single-particle wave functions. In this paper it is shown that the interaction kernel of CMWP can be expressed by using the nucleon-distribution functions instead of using the many-body wave function itself. This fact gives us a hint to understand intuitively the properties of the nucleus-nucleus interaction. And then we investigate the origin of the angular momentum and incident-energy dependence together with discussing the features of the distribution functions.

In Sec. II we briefly review the CMWP method and show the relation between the nucleon-distribution functions and the nucleus-nucleus interaction. In Sec. III some comments on the nucleon-nucleon effective interaction are made. In Sec. IV we discuss the nature of the density-distribution function and the Hartree-type-interaction kernel. In Sec. V we discuss phase-space distribution function and the Fock-type-interaction kernel. (These two-types of interaction kernels are defined in Sec. II.) In Sec.VI we show the numerical results on the nucleus-nucleus interactions by the CMWP method. Section VII is devoted to the summary and the concluding remarks.

Finally, it is noted here that in this paper all the considerations are performed on the assumption that both the projectile and the target are spin-isospin-saturated closed-shell nuclei. The systems explicitly treated are α-^{16}O and ^{16}O-^{16}O systems.

II. NUCLEUS-NUCLEUS INTERACTION BY THE CMWP METHOD

A. Brief review of the CMWP method

The nucleus-nucleus interaction $\mathcal{V}$ of CMWP is composed of the kinetic-exchange kernel $T_{\rm ex}$ and the interaction kernel V. They are given by the following expression:

$$\mathcal{V}(\mathbf{R},\mathbf{P})=T_{\rm ex}(\mathbf{R},\mathbf{P})+V(\mathbf{R},\mathbf{P}) , \tag{2.1}$$

$$T_{\rm ex}(\mathbf{R},\mathbf{P})=\left\langle \sum_{a=1}^{A+B}\hat{t}_a-\hat{T}_G\right\rangle-\frac{\mathbf{P}^2}{2\mu m}-(t_{\rm int}^{(A)}+t_{\rm int}^{(B)}+\tfrac{3}{4}\hbar\omega) , \tag{2.2}$$

$$V(\mathbf{R},\mathbf{P})=\left\langle \tfrac{1}{2}\sum_{a,b=1}^{A+B}\hat{v}_{ab}\right\rangle-(v_{\rm int}^{(A)}+v_{\rm int}^{(B)}) , \tag{2.3}$$

where $\hat{t}_a$, $\hat{T}_G$, μ, and $\hat{v}_{ab}$ are the kinetic-energy operator of each nucleon, the kinetic-energy operator of the center-of-mass motion, the reduced mass number of the nucleus-nucleus system, and the nucleon-nucleon effective interaction, respectively. The scalars $t_{\rm int}^{(\alpha)}$ and $v_{\rm int}^{(\alpha)}$ $(\alpha=A,B)$ are the kinetic- and interaction-internal energies. The term $\frac{3}{4}\hbar\omega$ is required because of using a Gaussian function as a wave function of the nucleus-nucleus relative motion. The expectation values of the operators are defined as

$$\langle\hat{O}\rangle=\frac{\langle\mathbf{Z}|\hat{O}|\mathbf{Z}\rangle}{\langle\mathbf{Z}|\mathbf{Z}\rangle} . \tag{2.4}$$

The many-body wave function in the center-of-mass system is defined as

$$|\mathbf{Z}\rangle=\left|\mathcal{A}\left[\phi_1\left[\mathbf{r}_1-\frac{1}{A}\sqrt{\mu/\nu}\mathbf{Z}\right]\ldots\phi_A\left[\mathbf{r}_A-\frac{1}{A}\sqrt{\mu/\nu}\mathbf{Z}\right]\right.\right.$$
$$\left.\left.\times\phi_{A+1}\left[\mathbf{r}_{A+1}+\frac{1}{B}\sqrt{\mu/\nu}\mathbf{Z}\right]\ldots\phi_{A+B}\left[\mathbf{r}_{A+B}+\frac{1}{B}\sqrt{\mu/\nu}\mathbf{Z}\right]\right]\exp\left[\frac{\mathbf{Z}^2}{2}\right]\right\rangle , \tag{2.5}$$

where ϕ_a $(a=1,\ldots,A+B)$ are the spatial and spin-isospin parts of the single-particle wave functions in the nuclei A and B. The harmonic-oscillator construction potentials are employed to get those wave functions. The operator $\mathcal{A}$ is the antisymmetrizer throughout the whole system. The oscillator width parameters for both nuclei are assumed to be equal in this study. The letters A and B are used not only to distinguish the target and the projectile but also to indicate the mass number of each nucleus. The definition of $\mathbf{Z}$ is

$$\mathbf{Z}=\frac{1}{\sqrt{2}}\left[\sqrt{2\nu\mu}\mathbf{D}+\frac{i}{\sqrt{2\nu\mu}}\frac{\mathbf{K}}{\hbar}\right] , \tag{2.6}$$

$$\nu=\frac{m\omega}{2\hbar} . \tag{2.7}$$

The vectors $\mathbf{D}$ and $\mathbf{K}$ are the noncanonical distance and momentum vectors, respectively, and have no direct physical meanings. The physical distance vector $\mathbf{R}$ and the physical momentum vector $\mathbf{P}$ are defined as

$$\mathbf{R}=\mathbf{D}\left|\frac{\partial}{\partial s}\ln\mathcal{N}(s)\right|^{1/2} ,$$
$$\mathbf{P}=\mathbf{K}\left|\frac{\partial}{\partial s}\ln\mathcal{N}(s)\right|^{1/2} ; \tag{2.8}$$

$$s=\bar{\mathbf{Z}}\mathbf{Z},\quad \mathcal{N}(s)=\langle\mathbf{Z}|\mathbf{Z}\rangle , \tag{2.9}$$

where the vector $\bar{\mathbf{Z}}$ is complex conjugate to $\mathbf{Z}$. It is noted that the norm $\mathcal{N}$ is a function depending only on the scalar product $s=\bar{\mathbf{Z}}\mathbf{Z}$.[4]

With these canonical variables $\mathbf{R}$ and $\mathbf{P}$, it is not hard to see that the Pauli-allowed region in the phase space of nucleus-nucleus relative motion is given by

$$\nu\mu\mathbf{R}^2+\frac{1}{4\nu\mu\hbar^2}\mathbf{P}^2\geq N_A . \tag{2.10}$$

The value N_A corresponds to the smallest quantum number of the RGM Pauli-allowed states.

The nucleus-nucleus interaction is given for each angular momentum l and incident energy E by determining the vectors $\mathbf{D}$ and $\mathbf{K}$ which satisfy the following equations:

$$\frac{1}{2\mu m}\mathbf{P}^2(\mathbf{D},\mathbf{K})+\mathcal{V}(\mathbf{R}(\mathbf{D},\mathbf{K}),\mathbf{P}(\mathbf{D},\mathbf{K}))=E ,$$
$$\mathbf{R}(\mathbf{D},\mathbf{K})\times\mathbf{P}(\mathbf{D},\mathbf{K})=\hbar\sqrt{l(l+1)} . \tag{2.11}$$

As a result, the nucleus-nucleus interaction begins to have the angular-momentum and incident-energy dependence.

The relationships between the canonical coordinates $\mathbf{R}$ and $\mathbf{P}$ and the noncanonical coordinates $\mathbf{D}$ and $\mathbf{K}$ are rather complicated. But here we show that those noncanonical and canonical vectors have a one-to-one correspondence with each other except at $\mathbf{D}=\mathbf{K}=0$. When the target and the projectile are both spin-isospin-saturated closed-shell nuclei, the norm $\mathcal{N}$ can be expanded in powers of s:

$$\mathcal{N}(s)=\sum_{N=0}^{\infty}\frac{\mu_N}{N!}s^N , \tag{2.12}$$

where μ_N are the eigenvalues of the RGM norm kernel and they are non-negative. As $\mu_0=0$ for the systems

treated in this paper, we get

$$\mathcal{N}(s)\geq 0 \ . \tag{2.13}$$

When $s=0$, that is, $\mathbf{D}=\mathbf{K}=0$, the norm $\mathcal{N}$ becomes 0. From Eq. (2.12) and the fact that μ_N are non-negative, it is obvious that the norm $\mathcal{N}$ and also the function $\ln\mathcal{N}$ are monotonic increasing functions of s. (For $\ln\mathcal{N}$, $s=0$ is the exception.) Then we can find that Eq. (2.8) is the one-to-one transformation. Therefore, the increase of $\mathbf{R}$ corresponds to the increase of $\mathbf{D}$, and the same for $\mathbf{P}$ and $\mathbf{K}$.

It is noted here that the kinetic-exchange kernel has no explicit angular momentum dependence. When we get the nucleus-nucleus interaction by self-consistent calculation with Eqs. (2.11), both the kinetic-exchange and interaction kernels produce the angular momentum dependence. However, as the angular momentum dependence has only the perturbative order of magnitude, it is essentially caused by only the parts which contain the scalar product $\mathbf{D}\cdot\mathbf{K}$. It is shown in Appendix A that the kinetic-exchange kernel can be written as follows:

$$T_{\rm ex}=\frac{\hbar^2\nu}{2m}[(\bar{\mathbf{Z}}\bar{\mathbf{Z}})+(\mathbf{Z}\mathbf{Z})]\frac{\partial}{\partial s}\ln(\mathcal{N}(s)e^{-s}) \ . \tag{2.14}$$

From the definitions of $\mathbf{Z}$ and $\bar{\mathbf{Z}}$ (2.6) and s (2.9), it is easy to see that the kinetic-exchange kernel (2.14) does not have the explicit angular momentum dependence. Therefore, it can be said that the angular momentum dependence of the nucleus-nucleus interaction is essentially caused by only the interaction kernel.

In the subsequent subsection we explain the structure of the interaction kernel more elaborately.

B. Interaction kernel of the CMWP method

When the target and the projectile are both spin-isospin-saturated closed-shell nuclei, the interaction kernel can be written in the form

$$\begin{aligned}
V(\mathbf{R},\mathbf{P})&=V_H+V_F-(v_{\rm int}^{(A)}+v_{\rm int}^{(B)}) \ , \\
V_H&=8\sum_{ijkl\in A,B}\int d\mathbf{r}_1 d\mathbf{r}_2\bar{\psi}_i(\mathbf{r}_1)\bar{\psi}_j(\mathbf{r}_2)v_d(\mathbf{r}_1-\mathbf{r}_2) \\
&\quad\times\psi_k(\mathbf{r}_1)\psi_l(\mathbf{r}_2)B_{ki}^{-1}B_{lj}^{-1} \ , \\
V_F&=8\sum_{ijkl\in A,B}\int d\mathbf{r}_1 d\mathbf{r}_2\psi_i(\mathbf{r}_1)\bar{\psi}_j(\mathbf{r}_2)v_e(\mathbf{r}_1-\mathbf{r}_2) \\
&\quad\times\psi_k(\mathbf{r}_1)\psi_l(\mathbf{r}_2)B_{kj}^{-1}B_{li}^{-1} \ ,
\end{aligned} \tag{2.15}$$

where ψ_i are the spatial parts of the single-particle wave functions ϕ_a. While the subscript a runs from 1 to $(A+B)$, the subscript i from 1 to $(A+B)/4$. B is the overlap matrix

$$B_{ij}=\langle\psi_i|\psi_j\rangle \quad (i,j\in A,B) \ . \tag{2.16}$$

The nucleon-nucleon interactions v_d and v_e are the direct and exchange interactions and are given by the following combinations of the state dependence of the effective interaction:

$$\begin{aligned}
v_d&=\tfrac{1}{16}[v(^1O)+3v(^3E)+3v(^1E)+9v(^3O)] \ , \\
v_e&=\tfrac{1}{16}[-v(^1O)+3v(^3E)+3v(^1E)-9v(^3O)] \ .
\end{aligned} \tag{2.17}$$

It is noted again that these combinations appear only when the target and the projectile are spin-isospin-saturated closed-shell nuclei. Hereafter the kernels V_H and V_F in the above expressions are abbreviated as the Hartree-type and Fock-type kernel, respectively.

The density-distribution function $\rho(\mathbf{r})$ of the nucleus-nucleus system is defined as

$$\rho(\mathbf{r})=4\sum_{ij\in A,B}\bar{\psi}_i(\mathbf{r})\psi_j(\mathbf{r})B_{ji}^{-1} \ . \tag{2.18}$$

Using this definition, the Hartree-type kernel V_H can be rewritten as

$$\begin{aligned}
V_H&=\frac{1}{2}\int\left[4\sum_{ik}\bar{\psi}_i(\mathbf{r}_1)\psi_k(\mathbf{r}_1)B_{ki}^{-1}\right]v_d(\mathbf{r}_1-\mathbf{r}_2) \\
&\quad\times\left[4\sum_{jl}\bar{\psi}_j(\mathbf{r}_2)\psi_l(\mathbf{r}_2)B_{lj}^{-1}\right] \\
&=\tfrac{1}{2}\int d\mathbf{r}_1 d\mathbf{r}_2\rho(\mathbf{r}_1)v_d(\mathbf{r}_1-\mathbf{r}_2)\rho(\mathbf{r}_2) \ .
\end{aligned} \tag{2.19}$$

The phase-space distribution function $f(\mathbf{r},\mathbf{p})$ (Wigner function) of the nucleus-nucleus system is defined as follows:

$$f(\mathbf{r},\mathbf{p})=4\sum_{ij\in A,B}\int d\mathbf{s}\,\bar{\psi}_i\left[\mathbf{r}+\frac{\mathbf{s}}{2}\right]\psi_j\left[\mathbf{r}-\frac{\mathbf{s}}{2}\right]B_{ji}^{-1}e^{i\mathbf{p}\mathbf{s}} \ . \tag{2.20}$$

Using this expression of f, we can get another expression for the Fock-type kernel V_F:

$$\begin{aligned}
V_F&=\frac{1}{2}\int\left[4\sum_{il}\bar{\psi}_i(\mathbf{r}_1)\psi_l(\mathbf{r}_2)B_{li}^{-1}\right]v_e(\mathbf{r}_1-\mathbf{r}_2)\left[4\sum_{jk}\bar{\psi}_j(\mathbf{r}_2)\psi_k(\mathbf{r}_1)B_{kj}^{-1}\right] \\
&=\frac{1}{2}\int d\mathbf{r}_1 d\mathbf{r}_2\frac{d\mathbf{p}_1 d\mathbf{p}_2}{(2\pi\hbar)^6}f\left[\frac{\mathbf{r}_1+\mathbf{r}_2}{2},\mathbf{p}_1\right][v_e(\mathbf{r}_1-\mathbf{r}_2)e^{-(i/\hbar)(\mathbf{p}_1-\mathbf{p}_2)\cdot(\mathbf{r}_1-\mathbf{r}_2)}]f\left[\frac{\mathbf{r}_1+\mathbf{r}_2}{2},\mathbf{p}_2\right] \\
&=\frac{1}{2}\int d\mathbf{r}\frac{d\mathbf{p}_1 d\mathbf{p}_2}{(2\pi\hbar)^6}f(\mathbf{r},\mathbf{p}_1)\bar{v}_e(\mathbf{p}_1-\mathbf{p}_2)f(\mathbf{r},\mathbf{p}_2) \ ,
\end{aligned} \tag{2.21}$$

where use has been made of the relation

$$4\sum_{ij\in A,B}\bar{\psi}_i(\mathbf{r}_1)\psi_j(\mathbf{r}_2)B_{ji}^{-1}=\int d\frac{d\mathbf{p}}{(2\pi)^3}f\left[\frac{\mathbf{r}_1+\mathbf{r}_2}{2},\mathbf{p}\right]e^{-i\mathbf{p}(\mathbf{r}_1-\mathbf{r}_2)}\ . \tag{2.22}$$

The effective interaction $\tilde{v}_e$ is an exchange interaction represented in the momentum space:

$$\tilde{v}_e(\mathbf{p})=\int dr\, v_e(\mathbf{r})e^{i\mathbf{p}\mathbf{r}}\ . \tag{2.23}$$

From Eqs. (2.19) and (2.21), it is found that the interaction kernel V_H is a sum of the nucleon-nucleon interactions in coordinate space and that V_F is the one in momentum space.

According to the kernel-classification method,[7] we decompose the interaction kernel into four parts, that is, *a*-, *b*-, *c*-, and *d*-type kernels. These types of kernels are defined as

$$\begin{aligned}
&(a\text{-type})\sim\langle\psi^{(A)}\psi^{(A)}|v_{d,e}|\psi^{(A)}\psi^{(A)}\rangle,\ \langle\psi^{(B)}\psi^{(B)}|v_{d,e}|\psi^{(B)}\psi^{(B)}\rangle,\ \langle\psi^{(A)}\psi^{(A)}|v_{d,e}|\psi^{(B)}\psi^{(B)}\rangle \text{ and c.c.}\ ,\\
&(b\text{-type})\sim\langle\psi^{(A)}\psi^{(B)}|v_{d,e}|v^{(A)}\psi^{(B)}\rangle\ ,\\
&(c\text{-type})\sim\langle\psi^{(A)}\psi^{(B)}|v_{d,e}|\psi^{(B)}\psi^{(A)}\rangle\ ,\\
&(d\text{-type})\sim\langle\psi^{(A)}\psi^{(A)}|v_{d,e}|\psi^{(A)}\psi^{(B)}\rangle \text{ and c.c.},\ \langle\psi^{(A)}\psi^{(B)}|v_{d,e}|\psi^{(B)}\psi^{(B)}\rangle \text{ and c.c.}
\end{aligned} \tag{2.24}$$

By the above definition of the classification, each type of the Hartree-type kernel V_H is written as

$$\begin{aligned}
V_H^a&=\frac{1}{2}\int d\mathbf{r}_1d\mathbf{r}_2v_d(\mathbf{r}_1-\mathbf{r}_2)[\rho_{AA}(\mathbf{r}_1)\rho_{AA}(\mathbf{r}_2)+\rho_{AB}(\mathbf{r}_1)\rho_{AB}(\mathbf{r}_2)+\rho_{BA}(\mathbf{r}_1)\rho_{BA}(\mathbf{r}_2)+\rho_{BB}(\mathbf{r}_1)\rho_{BB}(\mathbf{r}_2)]\ ,\\
V_H^b&=\int d\mathbf{r}_1d\mathbf{r}_2v_d(\mathbf{r}_1-\mathbf{r}_2)\rho_{AA}(\mathbf{r}_1)\rho_{BB}(\mathbf{r}_2)\ ,\\
V_H^c&=\int d\mathbf{r}_1d\mathbf{r}_2v_d(\mathbf{r}_1-\mathbf{r}_2)\rho_{AB}(\mathbf{r}_1)\rho_{BA}(\mathbf{r}_2)\ ,\\
V_H^d&=\int d\mathbf{r}_1d\mathbf{r}_2v_d(\mathbf{r}_1-\mathbf{r}_2)[\rho_{AA}(\mathbf{r}_1)\rho_{AB}(\mathbf{r}_2)+\rho_{AA}(\mathbf{r}_1)\rho_{BA}(\mathbf{r}_2)+\rho_{AB}(\mathbf{r}_1)\rho_{BB}(\mathbf{r}_2)+\rho_{BA}(\mathbf{r}_1)\rho_{BB}(\mathbf{r}_2)]\ .
\end{aligned} \tag{2.25}$$

And each type of the Fock-type kernel V_F is written as

$$\begin{aligned}
V_F^a&=\frac{1}{2}\int d\mathbf{r}\frac{d\mathbf{p}_1d\mathbf{p}_2}{(2\pi\hbar)^6}\tilde{v}_e(\mathbf{p}_1-\mathbf{p}_2)[f_{AA}(\mathbf{r},\mathbf{p}_1)f_{AA}(\mathbf{r},\mathbf{p}_2)+f_{AB}(\mathbf{r},\mathbf{p}_1)f_{AB}(\mathbf{r},\mathbf{p}_2)\\
&\qquad+f_{BA}(\mathbf{r},\mathbf{p}_1)f_{BA}(\mathbf{r},\mathbf{p}_2)+f_{BB}(\mathbf{r},\mathbf{p}_1)f_{BB}(\mathbf{r},\mathbf{p}_2)]\ ,\\
V_F^b&=\int d\mathbf{r}\frac{d\mathbf{p}_1d\mathbf{p}_2}{(2\pi\hbar)^6}\tilde{v}_e(\mathbf{p}_1-\mathbf{p}_2)f_{AB}(\mathbf{r},\mathbf{p}_1)f_{BA}(\mathbf{r},\mathbf{p}_2)\ ,\\
V_F^c&=\int d\mathbf{r}\frac{d\mathbf{p}_1d\mathbf{p}_2}{(2\pi\hbar)^6}\tilde{v}_e(\mathbf{p}_1-\mathbf{p}_2)f_{AA}(\mathbf{r},\mathbf{p}_1)f_{BB}(\mathbf{r},\mathbf{p}_2)\ ,\\
V_F^d&=\int d\mathbf{r}\frac{d\mathbf{p}_1d\mathbf{p}_2}{(2\pi\hbar)^6}\tilde{v}_e(\mathbf{p}_1-\mathbf{p}_2)[f_{AA}(\mathbf{r},\mathbf{p}_1)f_{AB}(\mathbf{r},\mathbf{p}_2)+f_{AA}(\mathbf{r},\mathbf{p}_1)f_{BA}(\mathbf{r},\mathbf{p}_2)\\
&\qquad+f_{AB}(\mathbf{r},\mathbf{p}_1)f_{BB}(\mathbf{r},\mathbf{p}_2)+f_{BA}(\mathbf{r},\mathbf{p}_1)f_{BB}(\mathbf{r},\mathbf{p}_2)]\ ,
\end{aligned} \tag{2.26}$$

where $\rho_{\alpha,\beta}$ $(\alpha,\beta=A,B)$ and $f_{\alpha,\beta}$ $(\alpha,\beta=A,B)$ are defined as

$$\rho_{\alpha,\beta}(\mathbf{r})=4\sum_{i\in\alpha}\sum_{j\in\beta}\bar{\psi}_i(\mathbf{r})\psi_j(\mathbf{r})B_{ji}^{-1}\quad(\alpha,\beta=A,B)\ , \tag{2.27}$$

$$\begin{aligned}
f_{\alpha,\beta}(\mathbf{r},\mathbf{p})=4\sum_{i\in\alpha}\sum_{j\in\beta}\int d\mathbf{s}\,\bar{\psi}_i\left[\mathbf{r}+\frac{\mathbf{s}}{2}\right]\\
\times\psi_j\left[\mathbf{r}-\frac{\mathbf{s}}{2}\right]B_{ji}^{-1}e^{i\mathbf{p}\mathbf{s}}\\
(\alpha,\beta=A,B)\ .
\end{aligned} \tag{2.28}$$

By definitions,

$$V_H=V_H^a+V_H^b+V_H^c+V_H^d\ , \tag{2.29}$$

$$V_F=V_F^a+V_F^b+V_F^c+V_F^d\ , \tag{2.30}$$

$$\rho(\mathbf{r})=\rho_{AA}(\mathbf{r})+\rho_{AB}(\mathbf{r})+\rho_{BA}(\mathbf{r})+\rho_{BB}(\mathbf{r})\ , \tag{2.31}$$

$$f(\mathbf{r},\mathbf{p})=f_{AA}(\mathbf{r},\mathbf{p})+f_{AB}(\mathbf{r},\mathbf{p})+f_{BA}(\mathbf{r},\mathbf{p})+f_{BB}(\mathbf{r},\mathbf{p})\ . \tag{2.32}$$

While the functions ρ_{AA}, ρ_{BB}, f_{AA}, and f_{BB} are real quantities, the functions ρ_{AB}, ρ_{BA}, f_{AB}, and f_{BA} are complex. But ρ_{AB} and f_{AB} are complex conjugate to ρ_{BA} and f_{BA}, respectively. Then from Eqs. (2.19), (2.21), (2.31), and (2.32) it is found that the imaginary parts of ρ_{AB}, ρ_{BA}, f_{AB}, and f_{BA} make no contribution to the nucleus-nucleus interaction.

III. DIRECT AND EXCHANGE NUCLEON-NUCLEON EFFECTIVE INTERACTIONS

The realistic form factor of the nucleon-nucleon effective interaction, which is obtained from the bare nucleon-nucleon interaction on the basis of the Brueckner-Hartree-Fock method, resembles one of the bare interaction, though the former is more moderate than the latter. For the triplet-even and singlet-even states the effective interaction has the form factors which are strongly attractive in the medium range and are strongly repulsive in the core region. The form factor for the triplet-odd state has a weak attraction in the medium range and has a weak repulsion in the core region. For the singlet-odd state it is weakly repulsive in all regions.

Figure 1(a) shows the form factor of the direct interaction given by the Hasegawa-Nagata-Yamamoto force (HNY).[8,9] It also has the repulsion in the core region and the attraction in the medium region. It is noted that the v_d is an attractive interaction. It is easily understood by the fact, for example, that the direct potential with the HNY force is attractive. The direct potential for the systems in which both the target and the projectile are spin-isospin-saturated closed-shell nuclei is given as

$$V_{\rm dir}(\mathbf{R})=\int d\mathbf{r}_1 d\mathbf{r}_2 \rho_A(\mathbf{r}_1) v_d(\mathbf{R}-\mathbf{r}_1+\mathbf{r}_2)\rho_B(\mathbf{r}_2)\ , \qquad (3.1)$$

where ρ_A and ρ_B are the density-distribution functions for the target and the projectile.

Figure 1(b) shows the form factor of the exchange interaction given by HNY in momentum representation. In the region where the relative momentum between the interacting two nucleons are small, the attraction is strong. As the relative momentum gets higher, the interaction decreases its attraction and becomes even repulsive.

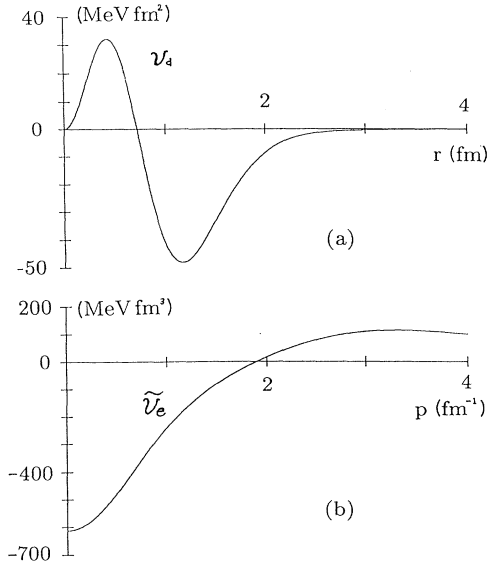

FIG. 1. The form factor of the direct interaction (a) and the exchange interaction (b) by the Hasegawa-Nagata-Yamamoto force. The Δ parameter in the HNY force is put to 21.3 MeV. The form factor of the direct interaction is multiplied by r^2.

IV. DENSITY-DISTRIBUTION FUNCTION AND HARTREE-TYPE-INTERACTION KERNEL

A. The features of the density-distribution functions

The densities ρ_{AA} and ρ_{BB} which include the overlap matrix elements of the nucleus-nucleus system differ from the densities (ρ_A,ρ_B) of the nuclei A and B. In the asymptotic region ($|\mathbf{R}|\to\infty$ or $|\mathbf{P}|\to\infty$) where the effects of the antisymmetrization disappear, the overlap matrix elements between the nuclei A and B become zero:

$$B_{ij}\to 0 \quad (i\in A,\ j\in B,\ |\mathbf{R}|\to\infty \text{ or } |\mathbf{P}|\to\infty)\ , \qquad (4.1)$$

and at the same time,

$$\rho_{AA}\to\rho_A,\ \rho_{BB}\to\rho_B \quad (|\mathbf{R}|\to\infty \text{ or } |\mathbf{P}|\to\infty)\ . \qquad (4.2)$$

The appearances of densities ρ_{AB} and ρ_{BA} originate from the antisymmetrization between the target and the projectile and they disappear in the asymptotic region:

$$\rho_{AB}\to 0,\ \rho_{BA}\to 0 \quad (|\mathbf{R}|\to\infty \text{ or } |\mathbf{P}|\to\infty)\ . \qquad (4.3)$$

Though near the Pauli-forbidden region,

$$\nu\mu\mathbf{R}^2+\frac{\mathbf{P}^2}{4\nu\mu\hbar^2}\sim N_A\ ,$$

the total density-distribution function ρ remains finite, all the components, ρ_{AA}, ρ_{AB}, ρ_{BA}, and ρ_{BB}, diverge. However, as we encounter such divergence only in the extremely low incident-energy region, the classification of the Hartree-type kernel (2.25) is not meaningless.

Figure 2 shows the density distribution in the scattering plane for the head-on colliding α-^{16}O system ($\mathbf{R}\|\mathbf{P}$). (The density-distribution and phase-space distribution functions are given in the center-of-mass system.) In the CMWP method the head-on collision corresponds to the

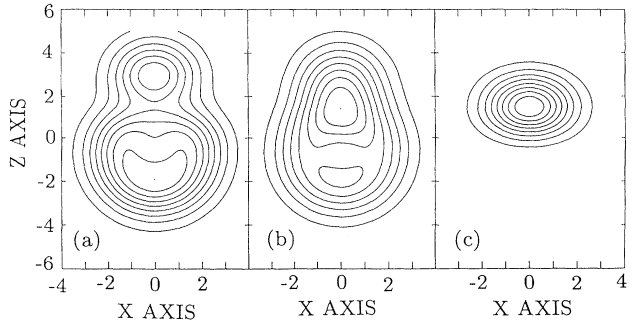

FIG. 2. The contour maps of the density-distribution functions for α-^{16}O system in case of the head-on collision. (a), (b), and (c) show ρ, $\rho_{AA}+\rho_{BB}$, and the real part of $\rho_{AB}+\rho_{BA}$, respectively. In this figure $|\mathbf{R}|=4.0$ fm, $|\mathbf{P}|=2.0$ fm^{-1}, and $\mathbf{P}$ is parallel to $\mathbf{R}$. The density-distribution functions ρ, ρ_{AA}, and ρ_{BB} are positive quantities, while the real parts of ρ_{AB} and ρ_{BA} are negative. The centers of ρ_{AA}, ρ_{BB}, and Reρ_{AB} (or Reρ_{BA}) located at $z=2.58$, $z=-0.65$, and $z=0.97$, respectively, where A is α and B is ^{16}O.

zero angular momentum. In this figure the relative distance $|\mathbf{R}|$ is 4.0 fm and the relative momentum $|\mathbf{P}|$ is 2.0 fm^{-1}. The oscillator parameter ν for this system is 0.1603 fm^{-2}. Figures 2(a)–2(c) show ρ, $\rho_{AA}+\rho_{BB}$, and real part of $\rho_{AB}+\rho_{BA}$, respectively. In this figure it is found that the densities ρ, ρ_{AA}, and ρ_{BB} are positive quantities but real parts of ρ_{AB} and ρ_{BA} are basically negative ones. ρ_{AB} and ρ_{BA} are located in the middle of the densities ρ_{AA} and ρ_{BB}. It is noted that ρ_{AB} and ρ_{BA} seen in Fig. 2(c) have something like an ellipsoidal shape and the direction of the long axis is perpendicular to the incident axis (z axis).

Figure 3 also shows the densities ρ, $\rho_{AA}+\rho_{BB}$, and real part of ρ_{AB} and ρ_{BA} for the α-^{16}O system. In this figure the absolute values of $\mathbf{R}$ and $\mathbf{P}$ are held fixed ($|\mathbf{R}|=4.0$ fm, $|\mathbf{P}|=2.0$ fm^{-1}), but the direction of vector $\mathbf{P}$ is perpendicular to the one of $\mathbf{R}$ ($\mathbf{R}\perp\mathbf{P}$). This corresponds to the situation in which the largest angular momentum within a given local momentum is realized. In this figure we put the direction of vector $\mathbf{R}$ parallel to the z axis and $\mathbf{P}$ parallel to the x axis. The features seen in this figure are almost the same as Fig. 2 except the shape of ρ_{AB} and ρ_{BA}. This time, ρ_{AB} and ρ_{BA} have round shapes. Comparing Fig. 2 with Fig. 3, we can find that the density-distribution functions ρ_{AB} and ρ_{BA} have the angular momentum dependence.

The same investigations are performed for the ^{16}O-^{16}O system (Figs. 4 and 5). The oscillator width parameter, relative distance $|\mathbf{R}|$, and relative momentum $|\mathbf{P}|$ are 0.1603 fm^{-2}, 6.0 fm, and 2.0 fm^{-1}, respectively. In Fig. 5 instead of the density-distribution functions themselves, the differences between the density-distributions for $\mathbf{R}\perp\mathbf{P}$ and the ones for $\mathbf{R}\parallel\mathbf{P}$ are shown. As shown in Fig. 5(b), the parts ρ_{AA} and ρ_{BB} as well as ρ_{AB} and ρ_{BA} have angular momentum dependence. This dependence is, however, negligibly small. From Figs. 5(a) and 5(c) it can be seen that the change of the total density ρ is almost equal to the one of ρ_{AB} and ρ_{BA}. The characteristic features for this system are almost the same as in the α-^{16}O system. Then it seems possible to say that those features of the density-distribution functions are quite general to the nucleus-nucleus systems.

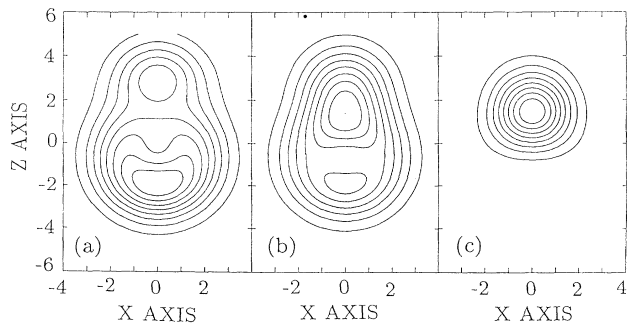

FIG. 3. Same as Fig. 2, but in this figure $\mathbf{P}$ is perpendicular to $\mathbf{R}$. Also in this figure the density-distribution functions ρ, ρ_{AA}, and ρ_{BB} are positive quantities, while the real parts of ρ_{AB} and ρ_{BA} are negative. The centers of ρ_{AA}, ρ_{BB}, and Reρ_{AB} (or Reρ_{BA}) located at $z=2.58$, $z=-0.65$, and $z=0.97$, respectively, where A is α and B is ^{16}O.

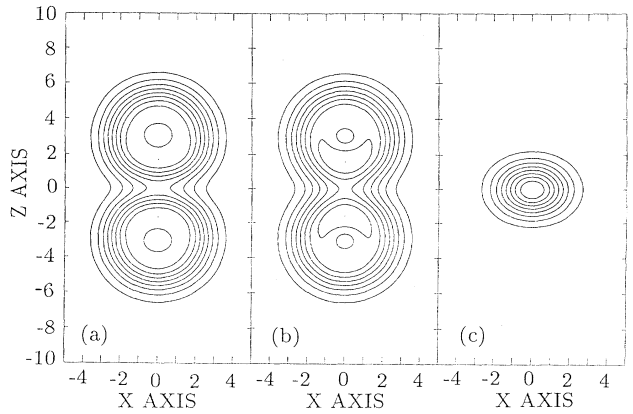

FIG. 4. The contour maps of the density-distribution functions for ^{16}O-^{16}O system in case of the head-on collision. (a), (b), and (c) show ρ, $\rho_{AA}+\rho_{BB}$, and real part of $\rho_{AB}+\rho_{BA}$, respectively. In this figure $|\mathbf{R}|=6.0$ fm, $|\mathbf{P}|=2.0$ fm^{-1}, and $\mathbf{P}$ is parallel to $\mathbf{R}$. The density-distribution functions ρ, ρ_{AA} and ρ_{BB} are positive quantities, while the real parts of ρ_{AB} and ρ_{BA} are negative. The centers of ρ_{AA}, ρ_{BB}, and Reρ_{AB} (or Reρ_{BA}) located at $z=2.93$, $z=-2.93$, and $z=0.0$, respectively.

B. Theoretical investigations on the Hartree-type-interaction kernel

From the above investigations on the structure of density-distribution functions and from the definition and the classification of the Hartree-type-interaction kernel Eq. (2.25), the following insight is deduced. As already mentioned, the nucleon-nucleon effective interaction v_d is attractive. And the densities ρ_{AA} and ρ_{BB} are positive quantities, but the densities ρ_{AB} and ρ_{BA} are negative. Then the a-, b-, and c-type kernels produce the attractive

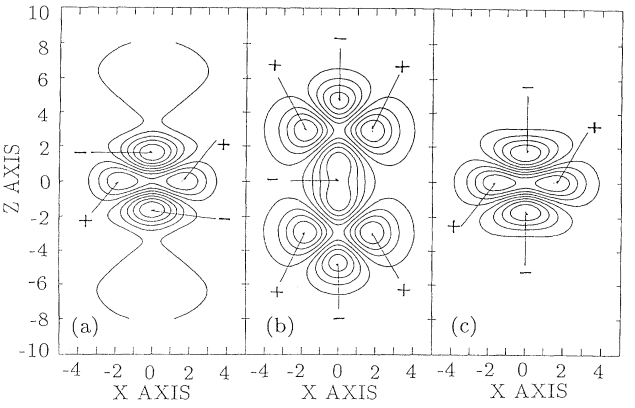

FIG. 5. The contour maps of the differences between the density-distribution functions for ^{16}O-^{16}O system in case of rotation and in case of head-on collision. This figure shows $\Delta\rho(l)=\rho(l)-\rho$ ($l=0$), and so on. (a), (b), and (c) show $\Delta\rho$, $\Delta\rho_{AA}+\Delta\rho_{BB}$, and the real part of $\Delta\rho_{AB}+\Delta\rho_{BA}$, respectively. In these figures $|\mathbf{R}|=6.0$ fm, $|\mathbf{P}|=2.0$ fm^{-1}, and $\mathbf{P}$ is perpendicular to $\mathbf{R}$. The symbols + and − in this figure indicate the positive and negative parts, respectively.

interaction to the nucleus-nucleus interaction, but the d-type kernel repulsive.

In the high incident-energy region the c-type and d-type kernels disappear and only the b-type and a part of a-type kernels remain. When the incident energy gets higher, the a-type and b-type kernels become closer to the interaction-internal energy and the direct potential, respectively. In the low incident-energy region, however, the former are different from the latter because of the effect of antisymmetrization.

The incident-energy dependence of the Hartree-type-interaction is brought by the one appearing in the density-distribution function, and it is caused only by the total antisymmetrization. Namely, the change of the Hartree-type kernel with the increase of the incident energy only traces to the disappearance of the effect of total antisymmetrization.

In the Hartree-type kernel the angular momentum dependence of the nucleus-nucleus interaction is expected to be produced mainly by the d-type kernel. When the angular momentum is equal to 0 ($\mathbf{R}\|\mathbf{P}$), the overlap of the densities ρ_{AA} and ρ_{BB} with the densities ρ_{AB} and ρ_{BA} becomes smallest. Then the repulsion of the d-type kernel also becomes weakest. When the angular momentum takes the maximum value ($\mathbf{R}\perp\mathbf{P}$), the densities ρ_{AB} and ρ_{BA} maximally overlap with the densities ρ_{AA} and ρ_{BB}. In this case the d-type kernel produces strongest repulsion. It is expected that the angular-momentum dependence of the Hartree-type-interaction kernel emerges as a decrease of the attraction with an increase of the relative angular momentum.[1,2]

V. PHASE-SPACE DISTRIBUTION FUNCTION AND FOCK-TYPE-INTERACTION KERNEL

A. The features of the phase-space distribution functions

Similar to the density-distribution functions, the phase-space distribution functions f_{AA} and f_{BB} differ from the one of each nucleus. In the asymptotic region the former become close to the latter:

$$f_{AA}\rightarrow f_A,\quad f_{BB}\rightarrow f_B\quad (|\mathbf{R}|\rightarrow\infty \text{ or } |\mathbf{P}|\rightarrow\infty)\,. \tag{5.1}$$

The appearances of the phase-space distribution functions f_{AB} and f_{BA} originate from the antisymmetrization between the target and the projectile and they disappear in the asymptotic region:

$$f_{AB}\rightarrow 0,\quad f_{BA}\rightarrow 0\quad (|\mathbf{R}|\rightarrow\infty \text{ or } |\mathbf{P}|\rightarrow\infty)\,. \tag{5.2}$$

Near the Pauli-forbidden region the total phase-space distribution function f remains finite, while the terms f_{AA}, f_{AB}, f_{BA}, and f_{BB} diverge. However, the definition of the classification of the Fock-type kernel (2.21) is meaningful except in the extremely low incident-energy region.

It is noted here that generally the functions f_{AA} and f_{BB} (and also f_A and f_B) do not have homogeneous structure and become positive at some point and negative at another point in the nucleon phase space. This fact is easily confirmed, for example, by calculating the phase-space distribution for one ^{16}O nucleus with the shell-model wave functions. This nature, which cannot be seen in classical systems, is the quantum fluctuation and originates from the Pauli blocking between the nucleons. But basically the functions f_{AA} and f_{BB} have to be considered as positive quantities. It is because ρ_{AA} and ρ_{BB}, which can be obtained from f_{AA} and f_{BB} by the integration on $\mathbf{p}$, are positive at each spatial point $\mathbf{r}$. As for the real parts of f_{AB} and f_{BA}, they are basically the negative quantities, because ρ_{AB} and ρ_{BA}, which can be also obtained from f_{AB} and f_{BA} by the integration on $\mathbf{p}$, are basically negative.

Figures 6 and 7 show the momentum distributions of nucleons for the head-on colliding α-^{16}O system ($\mathbf{R}\|\mathbf{P}$). The momentum distribution mentioned in this paper implies the distribution function given by the phase-space

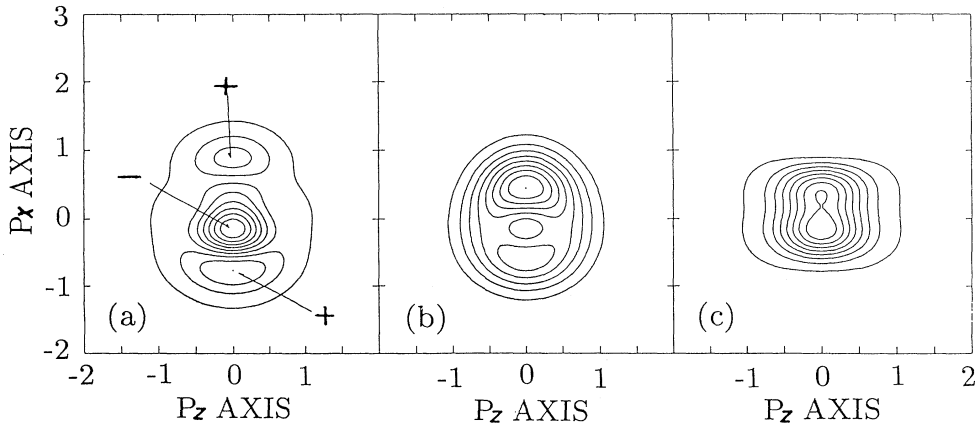

FIG. 6. The contour maps of the momentum-distribution functions for α-^{16}O system in case of the head-on collision. The momentum-distribution functions are given by the phase-space distribution function $f(\mathbf{r}_0,\mathbf{p})$, and so on. (a), (b), and (c) show f, $f_{AA}+f_{BB}$, and the real part of $f_{AB}+f_{BA}$, respectively. In these figures $|\mathbf{R}|=4.0$ fm, $|\mathbf{P}|=2.0$ fm^{-1}, and $\mathbf{P}$ is parallel to $\mathbf{R}$. $\mathbf{r}_0$ is $(x,y,z)=(0.0,0.0,0.97)$. The symbols + and − in this figure indicate the positive and negative parts, respectively. The momentum-distribution function f has the positive and negative parts, f_{AA} and f_{BB} are positive quantities, and the real parts of f_{AB} and F_{BA} are negative.

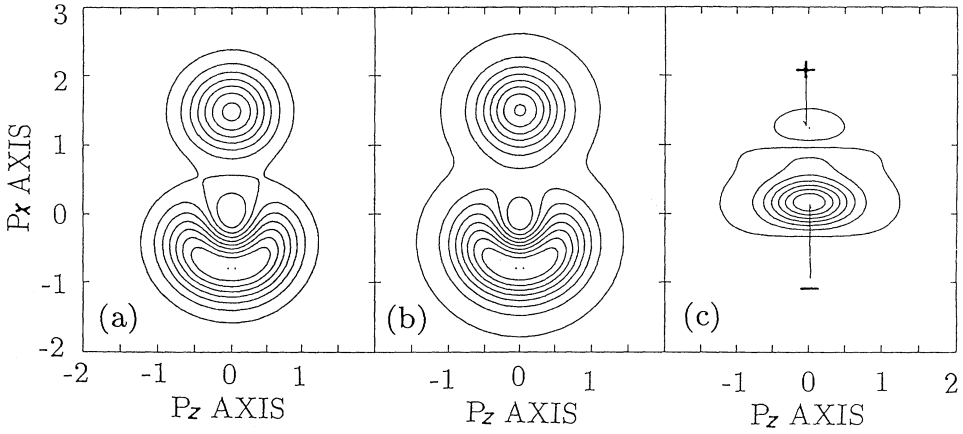

FIG. 7. Same as Fig. 6, but in this figure relative momentum $|\mathbf{P}|$ is 6.0 fm^{-1} which corresponds to the case of high relative momentum. In this figure $\mathbf{r}_0$ is $(x,y,z)=(0.0,0.0,1.20)$. The symbols + and − in this figure indicate the positive and negative parts, respectively. In this figure the momentum-distribution functions f, f_{AA}, and f_{BB} are positive quantities. The real parts of f_{AB} and f_{BA} are mainly negative but have small positive part.

distribution function at a fixed spatial point r_0, namely, it is given by $f(\mathbf{r}_0,\mathbf{p})$. For Fig. 6, we put $|\mathbf{R}|=4.0$ fm, $|\mathbf{P}|=2.0$ fm^{-1}, and $\mathbf{r}_0$ is taken to be the very middle of the centers of ρ_{AA} and ρ_{BB}. In Fig. 7 these parameters are the same as in Fig. 6 except $|\mathbf{P}|$. In Fig. 7 $|\mathbf{P}|$ is 6.0 fm^{-1} which corresponds to the case of high relative momentum.

Figures 6(a) and 7(a) show the total momentum distribution $f(\mathbf{r}_0,\mathbf{p})$. It is found that the maximum points in the distribution separate from each other with the increase of the relative momentum.

Figures 6(b) and 7(b) show $f_{AA}+f_{BB}$. From these figures it is confirmed that these functions are basically the positive quantities and that f_{AA} and f_{BB} separate from each other in the momentum space with the increase of the relative momentum.

Figures 6(c) and 7(c) show the real parts of f_{AB} and f_{BA}. Because the effect of the antisymmetrization vanishes in the high relative-momentum region, these functions disappear in that region. It is also confirmed here that these distribution functions are basically the negative quantities. And their centers are located in the middle of the distribution functions f_{AA} and f_{BB}.

The same investigations are performed for the ^{16}O-^{16}O system (Figs. 8 and 9). The parameters $|\mathbf{R}|$ and $|\mathbf{P}|$ are 6.0 fm and 2.0 fm^{-1} in Fig. 8 and 6.0 fm and 16.0 fm^{-1} in Fig. 9, respectively. And $\mathbf{r}_0$ is 0 in both figures. The characteristic features for this system are almost the same as seen in the α-^{16}O system. Then it seems possible to say that the features of the phase-space distribution functions shown in this section are quite general to the nucleus-nucleus systems.

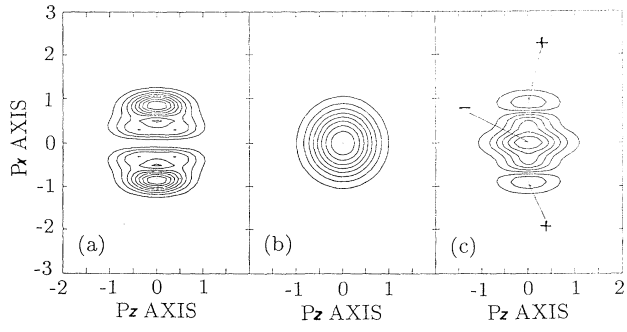

FIG. 8. The contour maps of the momentum-distribution functions for ^{16}O-^{16}O system in case of the head-on collision. (a), (b), and (c) show f, $f_{AA}+f_{BB}$, and the real part of $f_{AB}+f_{BA}$, respectively. In this figure $|\mathbf{R}|=6.0$ fm, $|\mathbf{P}|=2.0$ fm^{-1}, and $\mathbf{P}$ is parallel to $\mathbf{R}$. $\mathbf{r}_0$ is taken to be the middle of the centers of ρ_{AA} and ρ_{BB}, that is, $\mathbf{r}_0=0$. The symbols + and − in this figure indicate the positive and negative parts, respectively. In this figure the momentum-distribution functions f, f_{AA}, and f_{BB} are positive quantities. The real parts of f_{AB} and f_{BA} are mainly negative but have small positive part.

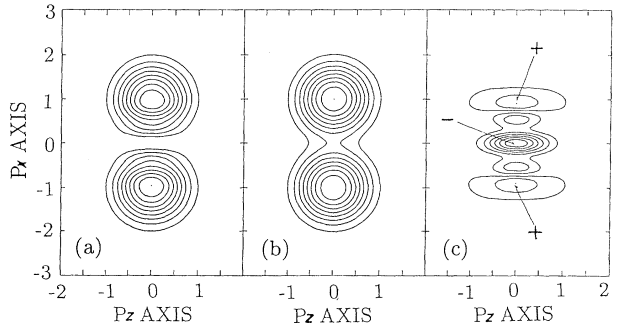

FIG. 9. Same as Fig. 8 but in this figure the relative momentum $|\mathbf{P}|$ is 16.0 fm^{-1} which corresponds to the case of high relative momentum. The symbols + and − in this figure indicate the positive and negative parts, respectively. Also in this figure the momentum-distribution functions f, f_{AA}, and f_{BB} are positive quantities. The real parts of f_{AB} and f_{BA} are mainly negative but have small positive part.

B. Theoretical investigations on the Fock-type interaction kernel

From the structure of the phase-space distribution functions shown in the above subsection and from the definition of each type of Fock-type kernel (2.26), we can expect the following qualitative features in Fock-type kernel.

As already mentioned in Sec. III, the exchange interaction v_e is attractive in low relative-momentum region. The phase-space distribution functions f_{AA} and f_{BB} are basically the positive quantities and $\mathrm{Re}f_{AB}$ and $\mathrm{Re}f_{BA}$ are negative. Therefore, the a-, b-, and c-type kernels produce the attraction to the nucleus-nucleus interaction, but the d-type kernel produces the repulsion.

In the high incident-energy region the b- and d-type kernels disappear and the remaining parts are the c-type kernel and a part of a-type kernel. In that region the c-type kernel becomes equal to the knock-on exchange potential and the a-type to the interaction-internal energy. In the low incident-energy region, however, the a-type and c-type kernels differ from the internal energy and the knock-on exchange potential because of the effects of antisymmetrization.

As for the incident-energy dependence, the behavior of the Fock-type kernel is expected to be different from the one of Hartree-type kernel. Though the incident-energy dependence of the Hartree-type kernel is brought only by the disappearance of the effects of antisymmetrization in the density-distribution function, the form factor of the exchange interaction as well as the antisymmetrization will make some contributions to the incident-energy dependence of the Fock-type kernel.

The c-type kernel is the interaction between the distribution functions f_{AA} and f_{BB} and these two distributions separate from each other with the increase of the relative momentum. Then in the high incident-energy region the attraction between these two parts becomes weak because the high-momentum part of the form factor of v_e is less attractive than in low relative momentum as seen in Fig. 1(b).

For the d-type kernel, the form factor of the exchange interaction plays the same kind of roles as expected in c type. The distance between f_{AA} and $\mathrm{Re}(f_{AB}+f_{BA})$ and the one between f_{BB} and $\mathrm{Re}(f_{AB}+f_{BA})$ become larger with the increase of the incident energy. Then, the repulsion of d-type kernel becomes weaker because of the decrease of the strength of exchange interaction. Moreover, the distributions f_{AB} and f_{BA} themselves vanish in the high incident-energy region. This vanishing promotes the behavior that the repulsion of d-type kernel weakens in the high incident-momentum region. Thus, the incident-energy dependence of d-type kernel is expected to be quite strong.

As for the angular momentum dependence of the Fock-type kernel, it is difficult to make definite statements on the basis of the investigation of the distribution functions and the effective interaction. However, it can be said that the d-type of the Fock-type kernel is also expected to bring the angular momentum dependence to the nucleus-nucleus interaction. The angular momentum dependence in the Hartree-type kernel originates from the change of the overlap of the parts ρ_{AA} and ρ_{BB} with the parts ρ_{AB} and ρ_{BA}. On the other hand, the density-distribution function can be given by the integration of the phase-space distribution function on momentum **p**. Then it is also expected that there is a change of overlap of the parts f_{AA} and f_{BB} with the parts f_{AB} and f_{BA}.

VI. NUMERICAL RESULTS ON NUCLEUS-NUCLEUS INTERACTION

In this section the nucleus-nucleus interactions obtained by the self-consistent calculation with Eqs. (2.11)

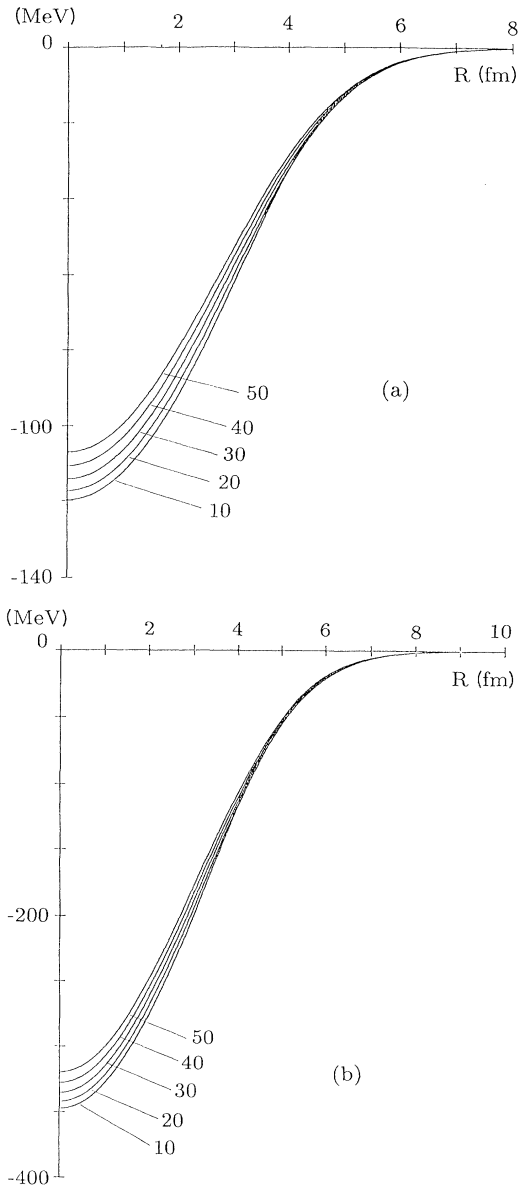

FIG. 10. Nucleus-nucleus interactions for α-^{16}O system (a) and ^{16}O-^{16}O system (b) in case of zero angular momentum. The numbers in these figures are the incident energies in units of MeV/nucleon.

are presented. All results are shown in the center-of-mass system and the incident energy is given in units of MeV/nucleon. The nucleon-nucleon effective interaction employed here is the HNY force introduced in Sec. III. The Δ parameter in the HNY force is taken as 21.3 MeV for α-^{16}O and ^{16}O-^{16}O systems.

The nucleus-nucleus interactions of s wave for α-^{16}O and ^{16}O-^{16}O systems are shown in Fig. 10. The strength of attraction for both cases becomes weaker with the increase of the incident energy. It is noted that this property does not appear without the antisymmetrization.

Volume integrals j_v of the above potentials and also the kinetic-exchange, Hartree-type-interaction, and Fock-type-interaction kernels are shown in Fig. 11. The definition of the volume integral is

$$j_v = \frac{1}{AB} \int d\mathbf{R}\, \mathcal{V}(\mathbf{R}) \,. \tag{6.1}$$

In this figure we show the volume integrals of Hartree-type and Fock-type kernels from which the internal energies are subtracted. First of all, for both systems it is found that the incident-energy dependence seen in Fig. 10 is produced by almost only the Fock-type-interaction kernel. Though the kinetic-exchange kernel also produces the incident-energy dependence to the nucleus-nucleus interaction, it is restricted in the quite low incident-energy region. The Hartree-type-interaction kernel makes no contribution to the incident-energy dependence. This fact implies that though there are no incident-energy dependence without the antisymmetrization, the incident-energy dependence caused by only the disap-

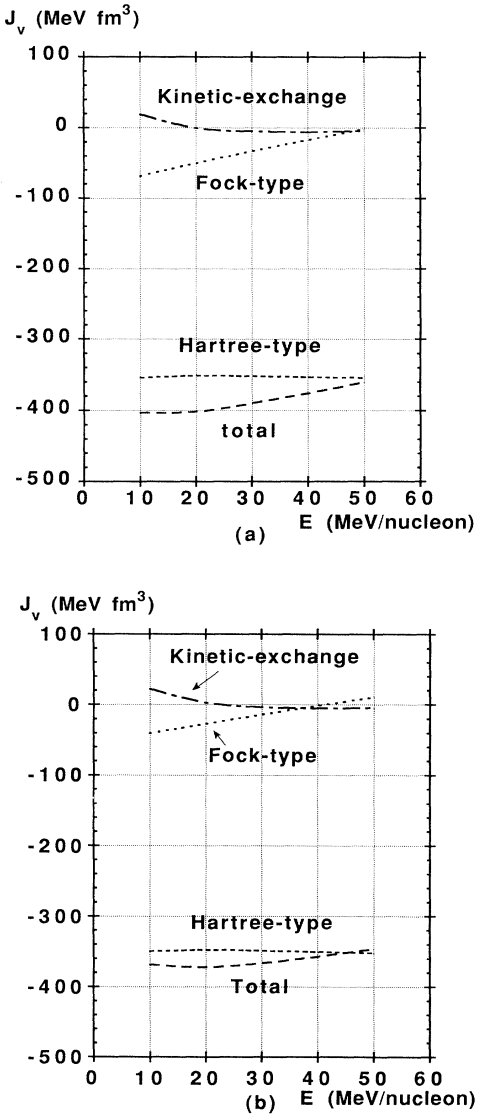

FIG. 11. Volume integrals of the nucleus-nucleus interaction, kinetic-exchange kernel, Hartree-type-interaction kernel, and Fock-type-interaction kernel for α-^{16}O system (a) and ^{16}O-^{16}O system (b) in case of zero angular momentum.

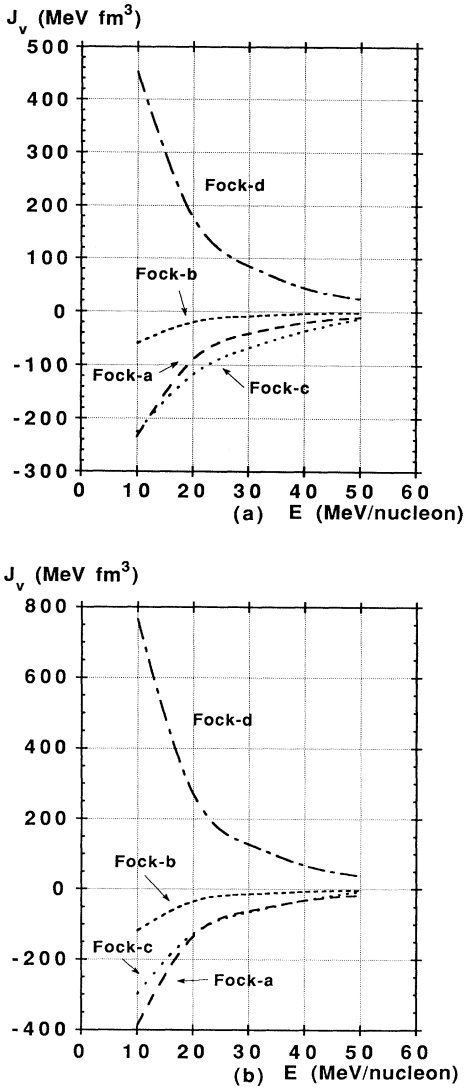

FIG. 12. Volume integrals of the Fock-a-, Fock-b-, Fock-c-, and Fock-d-type kernels for α-^{16}O system (a) and ^{16}O-^{16}O system (b) in case of zero angular momentum.

pearance of the effect of antisymmetrization is quite weak, and that the form factor of the exchange interaction plays an important role in the incident-energy dependence.

Figure 12 shows the volume intergals of Fock-*a*, -*b*, -*c*, -*d* type kernels. First of all, for α-^{16}O system below 20 MeV/nucleon there appears the influence of the divergence of phase-space distribution functions mentioned in Sec. V A. Above 20 MeV/nucleon it is clearly seen that the incident-energy dependence of the Fock-*d*-type kernel is largest among the four types of Fock kernels. One of Fock-*a*-type and Fock-*b*-type kernels is weak in this incident-energy region. The Fock-*c*-type kernel has the moderate incident-energy dependence in all the incident-energy regions and also has the second largest incident-energy dependence above 20 MeV/nucleon. As already mentioned in Sec. V B, the incident-energy dependence appearing in Fock-*a*-type and Fock-*b*-type kernels traces to the disappearance of the effect of antisymmetrization. On the other hand, the behavior of Fock-*c*- and Fock-*d*-type kernels is different from Fock-*a*- and Fock-*b*-type kernels. The incident-energy dependence of the former originates from not only the antisymmetrization but also the form factor of the exchange effective interaction. The fact that above 20 MeV/nucleon the incident-energy dependence of Fock-*c*-type and Fock-*d*-type kernels is larger than the one of Fock-*a*-type, and Fock-*b*-type kernels is the reflection of the effects of the form factor. For the ^{16}O-^{16}O system, though it is difficult to see the characteristic behavior of Fock-*c*-type kernel such as seen in the α-^{16}O system, the basic structures of the four types of Fock kernels are almost the same as the ones seen in the α-^{16}O system.

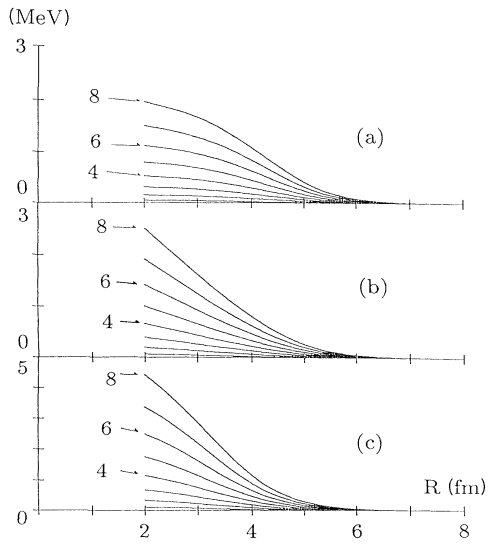

FIG. 13. Angular momentum dependence of the nucleus-nucleus interaction for α-^{16}O system which is expressed as the difference between the angular momentum l and the angular momentum 0: $\Delta V(l)=V(l)-V\ (l=0)$. (a), (b), and (c) show one of the total nucleus-nucleus interaction, the Hartree-type kernel, and the Hartree-*d*-type kernel, respectively. The numbers in this figure indicate the relative angular momentum. In this figure the angular momentum dependent nucleus-nucleus interactions are calculated without the parity projection.

Figures 13(a) and 14(a) show the angular momentum dependence of the nucleus-nucleus interactions for α-^{16}O and ^{16}O-^{16}O systems, respectively. The incident energy is 30 MeV/nucleon in each case. In these figures the angular momentum dependence are presented as the differences between the nucleus-nucleus interaction for angular momentum l and the one for zero angular momentum. It can be seen that in both systems the attraction of the nucleus-nucleus interactions weakens with the increase of the angular momentum.

Figures 13(b) and 14(b) show the angular momentum dependence of the Hartree-type-interaction kernels for α-^{16}O and ^{16}O-^{16}O systems, respectively. It is found that almost all the angular momentum dependence of the nucleus-nucleus interaction is explained by the one of the Hartree-type-interaction kernel. Though it is not shown numerically in this paper, the kinetic-exchange kernel and the Fock-type-interaction kernel do not make important contributions to the angular momentum dependence of the nucleus-nucleus interaction.

Figures 13(c) and 14(c) show the angular momentum dependence of the Hartree-*d*-type interaction kernels for α-^{16}O and ^{16}O-^{16}O systems, respectively. The angular momentum dependence of this kernel is larger than the one of the full nucleus-nucleus interaction seen in Figs. 13(a) and 14(a) or the one of Hartree-type-interaction kernels seen in Figs. 13(b) and 14(b). Though it is not shown, the parts canceling the angular momentum dependence of the Hartree-*d*-type kernel are the Hartree-*a*- and Hartree-*c*-type kernels. As well as the Hartree-*d*-type kernel, these types of kernels also include the density-distribution functions ρ_{AB} and ρ_{BA} whose shapes are transformed with the change of the angular momentum. And this brings the weak angular momentum dependence to the Hartree-*a*- and Hartree-*c*-type

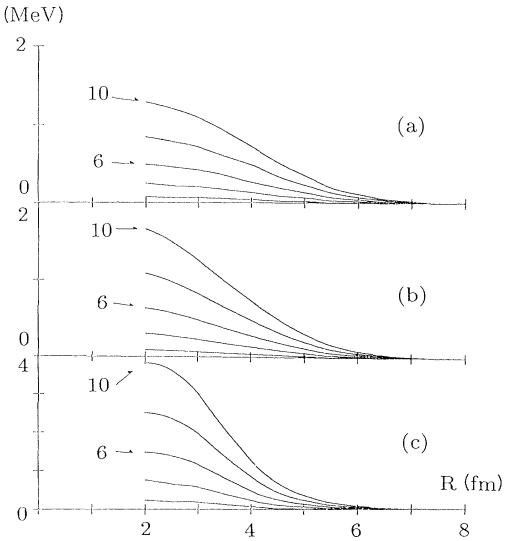

FIG. 14. Same as Fig. 13, but for ^{16}O-^{16}O system.

kernels. However, from these numerical results it may be said that essentially the Hartree-d-type-interaction kernel produces the angular-momentum dependence of the nucleus-nucleus interaction.

VII. SUMMARY AND CONCLUDING REMARKS

In this paper the efforts are concentrated on the investigation of the structure of nucleon distribution functions in order to get an intuitive understanding of the angular momentum and incident-energy dependence in the nucleus-nucleus interaction. Subject to employing a single Slater determinant as a many-body wave function, the interaction kernel of a many-body theory can be rewritten with the density- and phase-space distribution functions instead of employing the many-body wave function itself.

On the basis of the exchange characters, the nucleon distribution functions are decomposed into four parts, that is, ρ_{AA}, ρ_{AB}, ρ_{BA}, and ρ_{BB} for the density-distribution function and f_{AA}, f_{AB}, f_{BA}, and f_{BB} for the phase-space distribution function.

As for the density-distribution function, ρ_{AA} and ρ_{BB} are positive quantities. On the other hand, ρ_{AB} and ρ_{BA} are basically negative quantities. In contrast to ρ_{AA} and ρ_{BB}, the densities ρ_{AB} and ρ_{BA} vary their shapes with the increase of the angular momentum. The overlap of the densities ρ_{AA} and ρ_{BB} with the densities ρ_{AB} and ρ_{BA} becomes minimum at $l=0$. With the increase of the angular momentum this overlap becomes larger.

The phase-space distribution functions f_{AA} and f_{BB} are essentially positive quantities. On the other hand, f_{AB} and f_{BA} are basically negative quantities. While f_{AA} and f_{BB} separate from each other in momentum space with the increase of the relative momentum, f_{AB} and f_{BA} rest in the middle of f_{AA} and f_{BB}.

The angular momentum dependence of the nucleus-nucleus interaction is mainly produced by the Hartree-type-interaction kernel, especially by the Hartree-d-type kernel. The Hartree-d-type kernel is the interaction between the densities ρ_{AA} and ρ_{BB} and the densities ρ_{AB} and ρ_{BA}. As ρ_{AA} and ρ_{BB} are positive and ρ_{AB} and ρ_{BA} are negative, and, moreover, the direct effective interaction is attractive, then the Hartree-d-type kernel gives the repulsive contribution to the nucleus-nucleus interaction. As the overlap of the densities ρ_{AA} and ρ_{BB} with the densities ρ_{AB} and ρ_{BA} becomes larger when the angular momentum gets larger, then the repulsion of Hartree-d-type kernel becomes stronger. This nature emerges as the angular momentum dependence in the nucleus-nucleus interaction.

The incident-energy dependence of the nucleus-nucleus interaction is mainly produced by the Fock-type-interaction kernel. The Fock-a-, -b-, and -c-type kernels are attractive interactions and the strength of their attractions becomes weak with the increase of the relative momentum. On the other hand, the Fock-d-type kernel is repulsive and its repulsion becomes weak in the high relative-momentum region. The incident-energy dependence of the nucleus-nucleus interaction is composed of such behavior of these kernels. While the incident-energy dependence brought by the Fock-a- and Fock-b-type kernels only traces to the disappearance of the effect of antisymmetrization, the one by Fock-c- and Fock-d-type kernels traces not only to the disappearance of the effect of antisymmetrization but also to the form factor of the exchange effective interaction.

In this paper the investigation is restricted to systems in which both the target and the projectile are spin-isospin-saturated closed-shell nuclei. For other systems the kinetic-exchange kernel has explicit angular momentum dependence, and the other combinations of state dependence of the effective interaction in addition to the direct and exchange ones appear in the interaction kernel. However, it may be true of the other systems that the angular momentum dependence mainly originates from the Hartree-d-type kernel and that the incident-energy dependence in the wide range is basically produced by the Fock-type kernel. It is because the appearance of such dependence is essentially due to the effects of the antisymmetrization such as investigated in this paper.

On the question whether the characteristic features of nucleus-nucleus interaction investigated in this paper are peculiar to the many-body theory CMWP, it can be said that the same features are expected, for example, in the semiclassical version of the resonating-group method. It is already shown that the kernels of RGM+WKB are connected with the CMWP kernel by the simple transformation.[10] And also the numerical results given by these two methods coincide with each other quite well. Then it is natural to think that the structures of the nucleus-nucleus interaction discussed in this paper are commonly seen as the general features in the total-antisymmetrized many-body theories.

On the basis of the investigation in this paper the following two points should be noticed.

The structure of the distribution functions, such that some parts are positive and that other parts are negative, is obtained as a consequence of not only the antisymmetrization but also the proper treatment of the finiteness of the nucleus-nucleus system. The finiteness is taken into account by using the localized single-particle wave functions. Such statement seems to be a matter of course. However, for example, Izumoto *et al.* used the matter approach in the g-matrix calculation for the nucleus-nucleus systems.[11,12] Though their works are challenging and quite interesting, there may be the underestimation of the role of finiteness in their method. Although in nucleus-nucleus systems it is not known to what extent the proper treatment of finiteness is necessary or to what extent the matter approach is valid, it is important to take the effects of such finiteness into account properly in the microscopic studies based on the g-matrix theory.

The second point is on the incident-energy dependence. It is doubtless that there is a "dispersionlike" relation in the nucleus-nucleus interaction. More precisely, there are contributions of the dynamical polarization potential to the incident-energy dependence. However, the dispersion relation itself breaks down because of the antisymmetrization. And as shown in this paper, both the effects of total antisymmetrization and the realistic form factor of nucleon-nucleon effective interaction produce the large

incident-energy dependence in the nucleus-nucleus interaction. Then the studies[13–15] in which the dispersion relation is applied to the nucleus-nucleus interaction and where the attempts to explain the incident-energy dependence on the basis of the dispersion relation are made seem to be questionable. It is emphasized that care should be taken in the investigations of the basic natures of nucleus-nucleus interaction such as the incident-energy dependence.

In a forthcoming publication we will discuss the incident-energy dependence of the nucleus-nucleus interaction by the use of the total-antisymmetrized many-body theory and of the microscopic complex g matrix which has the density- and starting-energy dependence and which satisfies the dispersion relation.

ACKNOWLEDGMENTS

The author greatly appreciates Professor H. Horiuchi's advice and comments. This work was supported by the Grant-in-Aid for Scientific Research Fund from the Ministry of Education, Science and Culture (No. 02952035).

APPENDIX A

According to the method similar to the one appearing in Appendix A of Ref. 16, we can get the explicit formula for the kinetic-exchange kernel.

It is shown in Ref. 16 that when both the target and the projectile have SU(3)-scalar internal wave functions, we can get the following formula:

$$\langle Z|\sum_{a=1}^{A+B}(\mathbf{r}_a-\mathbf{R}_G)^2|Z\rangle=\left[\left\langle\sum_{a\in A}(\mathbf{r}_a-\mathbf{R}_A)^2\right\rangle_A+\left\langle\sum_{a\in B}(\mathbf{r}_a-\mathbf{R}_B)^2\right\rangle_B+\frac{3}{4\nu}+\frac{\mu}{4}(\bar{\mathbf{Z}}^2+\mathbf{Z}^2)\right]\mathcal{N}(s)+\frac{1}{2\nu}s\frac{\partial}{\partial s}\mathcal{N}(s)\ , \tag{A1}$$

$$\mathbf{R}_G=\frac{1}{A+B}\sum_{a=1}^{A+B}\mathbf{r}_a\ , \tag{A2}$$

$$\left\langle\sum_{a\in\alpha}(\mathbf{r}_a-\mathbf{R}_\alpha)^2\right\rangle_\alpha=\langle\phi_{\rm int}^\alpha|\sum_{a\in\alpha}(\mathbf{r}_a-\mathbf{R}_\alpha)^2|\phi_{\rm int}^\alpha\rangle\quad(\alpha=A,B)\ , \tag{A3}$$

$$\mathbf{R}_\alpha=\frac{1}{\alpha}\sum_{a\in\alpha}\mathbf{r}_a\quad(\alpha=A,B)\ , \tag{A4}$$

where $\phi_{\rm int}^\alpha$ $(\alpha=A,B)$ is the internal wave function of each nucleus.

What we must obtain this time is the analytical expression of $\langle\mathbf{Z}|\sum_{a\in A+B}\hat{t}_a-\hat{T}_g|\mathbf{Z}\rangle$. In order to get it we use the following relations:

$$\begin{aligned}&\langle V_{N,l}|\hat{P}^2_{\rm rel}|V_{N,l}\rangle=2\hbar^2\mu\nu(n+\tfrac{3}{2})\ ,\\&\langle V_{N-1,l}|\hat{P}^2_{\rm rel}|V_{N,l}\rangle=\hbar^2\mu\nu\sqrt{(N-1)(N+l+1)}\ ,\end{aligned} \tag{A5}$$

instead of

$$\begin{aligned}&\langle V_{N,l}|\mu R^2_{\rm rel}|V_{N,l}\rangle=\frac{1}{2\nu}(N+\tfrac{3}{2})\ ,\\&\langle V_{N-2,l}|\mu R^2_{\rm rel}|V_{N,l}\rangle=-\frac{1}{4\nu}\sqrt{(N-l)(N+l+1)}\ ,\end{aligned} \tag{A6}$$

As a result, we get the following formula:

$$\begin{aligned}&\langle\mathbf{Z}|\sum_{a=1}^{A+B}\hat{t}_a-\hat{T}_G|\mathbf{Z}\rangle\\&=\left[t_{\rm int}^{(A)}+t_{\rm int}^{(B)}+\frac{3\hbar^2\nu}{2m}-\frac{\hbar^2\nu}{2m}(\bar{\mathbf{Z}}^2+\mathbf{Z}^2)\right]\mathcal{N}(s)+\frac{\hbar^2\nu}{m}s\frac{\partial}{\partial s}\mathcal{N}(s)\ .\end{aligned} \tag{A7}$$

And we get the kinetic-energy kernel

$$\begin{aligned}T_{\rm ex}(\mathbf{R},\mathbf{P})&=\left\langle\sum_{a\in A,B}\hat{t}_a-\hat{T}_G\right\rangle-\frac{\mathbf{P}^2}{2\mu m}-(t_{\rm int}^{(A)}+t_{\rm int}^{(B)}+\tfrac{3}{4}\hbar\omega)\\&=\frac{\hbar^2\nu}{2m}(\bar{\mathbf{Z}}^2+\mathbf{Z}^2)\frac{\partial}{\partial s}\ln(\mathcal{N}(s)e^{-s})\ .\end{aligned} \tag{A8}$$

[1] K. Aoki, and H. Horiuchi, Prog. Theor. Phys. **69**, 857 (1983).
[2] T. Wada and H. Horiuchi, Phys. Rev. C **38**, 2063 (1988).
[3] M. Saraceno, P. Kramer, and F. Fernandez, Nucl. Phys. **A405**, 88 (1983).
[4] S. Yamaguchi, K. Yabana, and H. Horiuchi, Prog. Theor. Phys. **82**, 217 (1989).
[5] P. Kramer and M. Saraceno, *Geometry of the Time-Dependent Variational Principle in Quantum Mechanics*, Vol. 140 of *Lecture Notes in Physics* (Springer-Verlag, Berlin, 1981).
[6] T. Wada, S. Yamaguchi, and H. Horiuchi, Phys. Rev. C **41**, 160 (1990).
[7] M. LeMere, J. D. Stubeda, H. Horiuchi, and Y. C. Tang, Nucl. Phys. **A320**, 449 (1979).
[8] A. Hasegawa and S. Nagata, Prog. Theor. Phys. **45**, 1786 (1971).
[9] Y. Yamamoto, Prog. Theor. Phys. **52**, 471 (1974).
[10] K. Aoki and H. Horiuchi, Prog. Theor. Phys. **69**, 1154 (1983).
[11] T. Izumoto, S. Krewald, and A. Faessler, Nucl. Phys. **A341**, 319 (1980).
[12] A. Faessler, T. Izumoto, S. Krewald, and R. Sartor, Nucl.

Phys. **A359**, 509 (1981).
[13]M. A. Nagarajan, C. C. Mahaux, and G. R. Satchler, Phys. Rev. Lett. **54**, 1136 (1985).
[14]C. Mahaux, H. Ngo, and G. R. Satchler, Nucl. Phys. **A449**, 345 (1986).
[15]C. Mahaux, H. Ngo, and G. R. Satchler, Nucl. Phys. **A456**, 134 (1986).
[16]H. Horiuchi, T. Wada, and K. Yabana, Prog. Theor. Phys. **76**, 837 (1986).